The Journal of Physiology

https://jp.msubmit.net

JP-RP-2019-278661R2

Title: Wnts control membrane potential in mammalian cancer cells

Authors: Jonathan Ashmore
Hervør Olsen
Naja Sørensen
Christopher Thrasivoulou
Aamir Ahmed

Author Conflict: Aamir Ahmed: AA (principal inventor) and CT (co-inventor) have filed a patent for targeting Wnt signaling pathway for ß-catenin related disorders (New British Patent Application no. 1318659.8). Christopher Thrasivoulou: AA (principal inventor) and CT (co-inventor) have filed a patent for targeting Wnt signaling pathway for ß-catenin related disorders (New British Patent Application no. 1318659.8).

Author Contribution: Jonathan Ashmore: Acquisition or analysis or interpretation of data for the work; Drafting the work or revising it critically for important intellectual content; Final approval of the version to be published; Agreement to be accountable for all aspects of the work Hervør Olsen: Acquisition or analysis or interpretation of data for the work; Final approval of the version to be published; Agreement to be accountable for all aspects of the work Naja Sørensen: Acquisition or analysis or interpretation of data for the work; Final approval of the version to be published; Agreement to be accountable for all aspects of the work Christopher Thrasivoulou: Acquisition or analysis or interpretation of data for the work; Final approval of the version to be published; Agreement to be accountable for all aspects of the work Aamir Ahmed: Conception or design of the work; Acquisition or analysis or interpretation of data for the work;

Disclaimer: This is a confidential document.

Drafting the work or revising it critically for important intellectual content; Final approval of the version to be published; Agreement to be accountable for all aspects of the work

Running Title: Electrogenic Wnt signaling

Dual Publication: No

Funding: Prostate Cancer Research Centre charity: Aamir Ahmed, AA1

Disclaimer: This is a confidential document.

Wnts control membrane potential in mammalian cancer cells

Jonathan Ashmore[1], Hervør Olsen[2], Naja Sørensen[2], Christopher Thrasivoulou[3] and Aamir Ahmed[4]*

[1] Department of Neuroscience, Physiology and Pharmacology and UCL Ear Institute, University College London, Gower Street, London, WC1E 6BT, UK.

[2] Sophion Bioscience A/S, Baltorpvej 154 - DK-2750 Ballerup, Denmark.

[3] Research Department of Cell & Developmental Biology, Centre for Cell & Molecular Dynamics,Rockefeller Building, University Street,University College London, London WC1E 6JJ, UK.

[4] Centre for Stem Cells and Regenerative Medicine, King's College London, 28th Floor, Tower Wing, Guy's Hospital, Great Maze Pond, London SE1 9RT, UK and Prostate Cancer Research Centre, Division of Surgery, 3rd Floor Laboratories, Charles Bell House, 67 Riding House Street, University College London, London W1W 7EJ, UK.

*To whom correspondence should be addressed: aamir.ahmed@kcl.ac.uk

Address for correspondence:

Aamir Ahmed, Centre for Stem Cells and Regenerative Medicine, King's College London, 28th Floor, Tower Wing, Guy's Hospital, Great Maze Pond, London SE1 9RT, UK and
Prostate Cancer Research Centre, Division of Surgery, 3rd Floor Laboratories, Charles Bell House, 67 Riding House Street, University College London, London W1W 7EJ, UK.

Abstract: 143 words

Main text: 5349 words

Figure legends: 1676 words

Abstract

The Wnt signaling network determines gene transcription with free intracellular Ca^{2+} (Ca^{2+}_i) and ß-catenin as major intracellular signal transducers. Despite its critical importance during development and disease, many of the basic mechanisms of Wnt signal activation remain unclear. Here we show by single cell recording and simultaneous Ca^{2+}_i imaging in mammalian prostate cancer cells that an early step in the signal cascade is direct action on the cell membrane potential. We show that Wnt ligands 5A, 9B and 10B rapidly hyperpolarized the cells by activating K^+ current by Ca^{2+} release from intracellular stores. Medium-throughput multi-well recordings showed responses to Wnts at concentrations of 2 nM. We identify a putative target for early events as a TRPM channel. Wnts thus act as ligands for ion channel activation in mammalian cells and that membrane potential is an early indicator of control of transcription.

One Sentence Summary: Wnt proteins determine membrane potential in cancer cells on a sub-second time scale.

Key points

- Wnt ligands belonging to both canonical and non-canonical Wnt pathways regulate membrane potential signifying a very early event in the signal transduction.
- Wnts activate K^+ currents by elevating intracellular Ca^{2+} and trigger Ca^{2+} release from intracellular stores.
- Control of potential by Wnt ligands has significant implications for gene transcription and opens up a novel avenue to interfere with this critical pathway.

Key words: Wnt, cancer, prostate, PC3, Ca^{2+}, medium-throughput electophysiology, patch clamp.

Introduction

Wingless-related integration site (Wnt) ligands are conserved, cysteine-rich secreted proteins that act as close-range signaling molecules. Wnt signal activation initiates a complex downstream signal cascade in eukaryotic cells and is critical in development and many diseases, including cancer (Clevers & Nusse, 2012; Schwarz-Romond, 2012). Free intracellular calcium (Ca^{2+}_i) and ß-catenin, a 92 kDa transcription factor co-activator protein, are the two major downstream transducers thought to act via the non-canonical and canonical pathways in eukaryotic cells (Nusse, 2012). Multiple Wnts, belonging to both canonical and non-canonical Wnt pathways (e.g. 5A, 9B, 10B), also act in mammalian cells by first activating a pulse of Ca^{2+}_i from the stores which is correlated with a translocation of ß-catenin to the nucleus (Thrasivoulou *et al.*, 2013).

Wnt ligand interaction at the cell membrane has generally been investigated through phosphorylation of receptors and co-receptors (Frizzled, FZDs and Lipoprotein, LRPs) initiating an intracellular cascade involving phosphoproteins and kinases (Klaus & Birchmeier, 2008; Clevers & Nusse, 2012). The mechanism involves the cysteine rich domain (CKCXXXXXXCXXXXC) of Wnt proteins interacting with N-terminus of FZD receptor (Bourhis *et al.*, 2010). The timescale of such determinations is generally many minutes to hours (Andersson *et al.*, 2004; Zeng *et al.*, 2005; Bilic *et al.*, 2007) and does not provide the dynamic resolution necessary for detailed understanding of the temporal dimension of signal transduction (Grundmann & Kostenis, 2017). The time resolution of measurements of Wnt signal activation can be reduced to tens of seconds using measurement of Ca^{2+}_i release (Thrasivoulou et al., 2013; Narendra Talabattula et al., 2017) but this has still meant that mechanistic details, characteristic of ligand-receptor binding (Pastan & Willingham, 1981; Sklar *et al.*, 1984) and the very early events of Wnt ligand interaction at the cell membrane remain unresolved (Dijksterhuis *et al.*, 2014).

We have previously shown that canonical (eg. Wnt3A, Wnt9B and Wnt10B) and non-canonical Wnts (e.g Wnt5A) activate Ca^{2+}_i release and stabilize ß-catenin in cancer cell lines from human prostate, breast and bladder and simian kidney (Thrasivoulou *et al.*, 2013). These experiments suggest that Wnt activation may also alter the cell's electrical activity and might provide a biological assay that can provide enhanced temporal sensitivity. It is

known that a variety of ion channels and particularly K^+ channels are implicated in tumour initiation and progression (reviewed in (Pardo & Stuhmer, 2014) (Noyer *et al.*, 2018)). Ion channels, responding in much less than a second, operate on rapid time scales which could be critical for a detailed understanding of control and regulation of downstream signal transduction.

We show here that an early step in the Wnt signal cascade of both canonical and non-canonical Wnt ligands (here, 5A, 9B, 10B) in mammalian cancer cells is the control of the cell membrane potential. The initial effects are triggered within 100 ms of arrival of the Wnt ligands at the cell membrane. We show using multi-well medium throughput system that Wnt action at nanomolar levels initiates activation of a Ca^{2+}-dependent K^+ (K(Ca)) current, hyperpolarizing the cells, but that Ca^{2+} permeation through a non-selective pathway, identified as a TRP channel, can contribute to trigger Ca^{2+}_i release.

Such control of potential, in non-excitable cells as used here, is a new way of understanding the function and modulation of the Wnt pathway in relation to cell electrical potential. This understanding is particularly useful in diseases where the Wnt pathway is known to play a critical role (Clevers & Nusse, 2012)

Methods

Cell lines

PC3 and LnCaP, prostate cancer and MCF7 breast cancer cell lines were obtained from the American Type Culture Collection (ATCC) via John R W Masters, University College London and cultured in RPMI 1640 (Invitrogen, Paisley, UK) medium containing 5 mM L-glutamine and fetal bovine serum (FBS) as described elsewhere (Thrasivoulou *et al.*, 2013). Cells from available passages 9-37 (for MCF7 and PC3) and 79-89 (LnCaP) were used 48-72 hours after plating. Cells for study were chosen from non-confluent colonies.

Electrophysiology

QPatch medium-throughput voltage clamp

On the day of the experiment, cells were trypsinized, washed and transferred to a measuring plate (a 16 or 48 well QPlate) a central component of a medium-throughput

patch clamp system (QPatch, Sophion, Denmark). A single cell attaches to the patch hole in a well (planar patch-clamping) to achieve a gigaohm seal. The volume of each well in a QPlate is 200 µl and solutions can be changed completely in the well within 0.2s. After 2-5 min (stabilization) the cells enter a whole-cell patch configuration with the help of a pressure protocol. The 16 or 48 cells are measured in parallel (with individual amplifiers), with a gigaseal achieved in >90% of the cells. The mean capacitance of a typical sample of 48 stably recorded (>20 mins) cells was 29.1 pF, corresponding to a spherical cell 30 µm in diameter. The capacitance remained steady throughout the recording. Those wells where the stability was compromised, judged by the cell capacitance, were excluded from the analysis. The intracellular solution contained (in mM): $CaCl_2$, 5.3, $MgCl_2$, 1.7, EGTA, 10; HEPES, 10; KF, 100; KCl, 20 and Na_2ATP, 4; adjusted to pH 7.2 and osmolarity 295 mOsm. The intracellular solution is thus calculated to contain 68 nM free Ca^{2+}. In some experiments 120 mM intracellular K^+ was replaced by Cs^+ to block K^+ channels. The extracellular solution contained (in mM) NaCl, 145; KCl, 4; $CaCl_2$, 2; $MgCl_2$,1; HEPES, 10, adjusted to pH 7.4.

Single cell patch clamp

Cells were grown on sterile 13 mm diameter glass coverslips (Thermo Fisher, UK) and recordings were made using whole cell tight seal patch clamp using an Axon 200B amplifier (Molecular Devices, USA). No series resistance or capacitance compensation was used. Cells were held at 0 mV or at -25 mV (e.g. Figure 5A), with no adverse effects as it was found that the very large inward currents in these experiments rapidly curtailed the recording stability. The coverslips were placed in a 1.5 ml bath continuously perfused with extracellular solution at 37^{o}C. Cells were imaged using an upright LSM510 confocal microscope (Zeiss, Germany) equipped with a 63x WI 1.0 NA objective allowing for simultaneous electrical recording and live cell Ca^{2+} imaging.

The intracellular pipette solution was chosen to minimise any Cl^- leak and contained (in mM): K-gluconate, 140; $MgCl_2$, 1; Na_2ATP, 4; EGTA, 1; HEPES, 10 to pH 7.2. There was no significant difference in the currents if Cl^- replaced gluconate, indicating no Cl^- permeability was present in these cells, consistent with published results. Isotonic substitution of K^+ with Cs^+ was made in some experiments. The extracellular solution was identical to the Q-Patch experiments above.

Data were acquired using pClamp 10.6 and a Digidata 1440A interface (Molecular Devices, USA) sampling at 10 kHz, and an auxiliary Axoscope sampling at 1kHz for simultaneous continuous traces. Offline analysis was carried out using either Clampfit (Molecular Devices, USA) or purpose-written Matlab code (Mathworks, Natick, USA). A junction potential correction for the pipette intracellular solution was computed, using pClamp software, to be -14 mV.

Wnt and drug delivery

Wnts (5A, 9B and 10B, R&D Systems, Bio-Techne) were applied by pipetting either 0.75, 1 or 2 µl volumes into the bath approximately 1 -2 mm away from the cells. The estimated final bath concentrations from known Wnt stock supplies were 1.5, 2 or 4 nM, respectively. The concentration of the Wnts under the water dipping objective on the upright LSM510 confocal microscope was measured by the rise of a fluorescent dye Alexa647 (Life Technologies, UK) included with the ligands. The 633 nm laser line was used to excite the dye and a separate imaging channel recorded Alexa647 dye co-ejected with the Wnts. This allowed absolute calibration of the Wnt dose. The synchronization for the drug application and the electrical recording was produced by an interface establishing event markers on the imaging files.

Where timing was critical, solutions were applied locally around the cell using a puffer pipette, placed no more than 100 µm from the cell to be recorded (as in Figure 1). For such local application, a controlled pressure was applied to eject solutions (Picopump PV830, WPI). The bulk flow in these cases is not diffusion limited and thus any difference between the diffusion times of two molecules (Wnt and Alexa647) was not significant.

In other single cell experiments, a 2 µl bolus of Wnt, (chosen to reach 4 nM final concentration in the bath), was applied 1-2 mm from the cells. Such delivery, with complex mixing below the objective, produced a slow 50-100 s rise in the Wnt concentration to a peak which could exceed the final calculated bath concentration by over an order of magnitude. From a determination of the Alexa647 bulk concentration and comparing with the fluorescence at the imaging plane, we estimate that cells in these experiments were

transiently exposed to such Wnt concentrations. Iclin, menthol and BCTC ((N-(4-tertiarybutylphenyl)-4-(3-chloropyridin-2-yl)tetrahydropyrazine-1(2H)-carbox-amide)) were obtained from Sigma.

Simultaneous Ca^{2+}_i imaging with single cell patch clamp electrophysiology

Cells grown on glass coverslips were used as described above. For Wnt induced Ca^{2+}_i release the patch pipette also contained 200 μM of the low affinity (K_d =20 μM) Ca^{2+} dye OGB-5N (Life Technologies, UK), chosen to maximize the dynamic range of the Ca^{2+}_i release measurement. OGB-5N was excited by the 488 nm line of the confocal argon ion laser and the emitted fluorescence (500-550 nm) monitored, continuously, during dye loading. 512x512, 12 bit images were collected at 1 or 0.5 Hz and synchronised event triggers added to the image file. Routine mechanical stability over 30 min recording was improved by using a specifically designed pipette holder (Luigs & Neumann, Germany).

Data analysis

Regions of interest (ROI) were drawn over individual PC3 cells in a single frame and fluorescence intensity measurements were made using ImageJ or purpose written Matlab scripts. Most experiments were repeated in at least 3 different passages of cells and data for 5-59 cells were used for statistical analysis. Statistical significance was calculated using Mann Whitney U-test. Unless otherwise stated, statistical data are presented as mean ± SEM.

Results

Wnt activates short latency membrane potential changes

Figure 1 near here

The resting potential of PC3 cells, measured in current clamp was (-23.8 ± 2.5 mV, n=59 cells, Figure 1). Similar observations have been reported in previous studies of prostate cancer cells (Laniado *et al.*, 2001).

Figure 1 shows that PC3 cells responded to the local application of Wnts. Wnts were applied by a local puffer pipette brought up to the cell just before recording to avoid leaks or backflow. Wnts were applied by a local puff whilst recording. Application of the extracellular solution alone had no effect, ruling out a possible mechanical perturbation as the stimulus. The Wnt responses consisted of a short lasting depolarization (lasting 5-10 s) followed by a longer-lasting hyperpolarization. The depolarization amplitude was 4.6 ± 1.6 mV and 5.4 ± 1.4 mV for Wnt 5A and Wnt 9B respectively and a hyperpolarization of -12.7 ± 2.5 mV and -11.2 ± 4.6 (n= 9-19; Figure 1) respectively. The cellular response to Wnt rapidly desensitized, a second response to Wnt within the stable recording period (> 10 min) being either absent or significantly reduced. With prolonged pressure application of the Wnt ligand, the cell often irreversibly depolarized to near 0 mV, thus terminating the recording. The membrane potential experiments were therefore done on distinct cells (n=>40 for the two Wnt ligands).

Considering that two populations of K(Ca) channels are reported in PC3 cells (Laniado *et al.*, 2001), the simplest explanation for the above results is that Ca^{2+}_i was increased by Wnt application to activate K^+ currents. Experiments were therefore conducted with 5 mM EGTA perfused into the bath to reduce external Ca^{2+} to below 1 µM. Figure 1D shows that cells still responded with a hyperpolarization, (-16.5 ± 10.2 mV, n=4 individual cells), not significantly different from data with 2 mM normal external Ca^{2+}. These results show that the responses did not depend on an immediate influx of Ca^{2+}. Such observations are also consistent with imaging data where Ca^{2+}_i pulses produced by Wnts were measured with nominally 0 Ca^{2+} in the bath (Thrasivoulou *et al.*, 2013).

Time course of initial Wnt activation

Figure 2 near here

To determine the time course of the early events and dissect the mechanisms resulting from exposure to Wnts, single cell recording was combined with live Ca^{2+} imaging. To obtain a better time resolution, confocal line scans were employed to image the Ca^{2+}_i indicator OGB-5N loaded into the cells from the pipette (Figure 2). When Wnts (here shown for Wnt9B), were puff applied, the response consisted of a short depolarization followed by a hyperpolarization (as in Figure 1). The Ca^{2+}_i signal first decreased slightly ($|DF/F_o| < 0.1$) before increasing as the cell hyperpolarized. The time-resolved latency of the initial depolarization showed that the response occurred within 100 ms. This rapid and unexpected reduction suggests either that Ca^{2+}_i was actively buffered, or that Ca^{2+}_i was extruded from the cell, or that a small Ca^{2+}_i influx was being reduced. The issue is addressed below.

For those experiments where Wnt delivery was monitored by Alexa647, we performed control experiments (n=3 or more cells in each case) to show that puff application of Alexa647 alone had no detectable effects on membrane potential. Application of extracellular solution containing Alexa647 alone had no effect. Wnts, which had been inactivated by repeated freeze-store cycles (>6), likewise produced no change in membrane potential. These observations strongly suggest the ligand itself was responsible for the responses described above.

Currents induced by Wnt ligands in single cells

Figure 3 near here

We next analysed single cells under whole cell voltage clamp. Single PC3 cells exhibited a prominent outward rectification above +40 mV (Figure 3). This has been reported in other studies and arises from a K(Ca) current (Laniado *et al.*, 2001; Yan & Aldrich, 2010). However, Figure 3A shows that PC3 cells exhibited a small non-zero conductance around rest (slope conductance, 6.7 ± 1.4 nS at 0 mV, n=24). It should be noted that if subtracted data were used this feature would have been obscured. Figure 3 shows that PC3 cells exhibited a small mean holding current at 0 mV of +38.4 ±2.2 pA (n=40).

The low resting potential of PC3 cells and a variable resting conductance suggest that at least one other channel as well as K(Ca) was present, serving to shunt any endogenous K^+ currents. As reported in other studies, this was not due to Cl^- (Laniado *et al.*, 2001). The small resting potential suggests that a small cation permeability P_X is present in addition to the K^+ permeability, P_K due to any K(Ca) channels. (A short calculation suggests that a mean resting potential of -23 mV would have been consistent with $P_X/P_K \sim 0.5$).

When Wnts were applied to voltage clamped PC3 cells as a bolus, (Figure 3D-G), there was a significant increase of a conductance which slowly reversed. In a sample of 21 PC3 cells, the slope conductance at 0 mV increased from 6.1 ± 1.5 nS to 30.5 ± 4.4 nS after Wnt application.

Although other cancer cell lines were tested and responded to Wnts (Figure 3), not all cell lines had the same electrical profile. For example, Wnts also activated large currents in a breast cancer cell line MCF7 (Figure 3H-K). Another prostate cancer cell line, LnCaP, had a more negative mean resting potential (-38.7 ± 5.1 mV, n=16), but also showed Wnt-induced currents (Figure 3 L-O). The Wnt response thus appears to be a general property of these cells. Such data are consistent with activation by Wnts of Ca^{2+}_i release in numerous different cell types (Thrasivoulou *et al.*, 2013).

Currents produced by slow delivery of Wnts to PC3 cells

Figure 4 near here

Figure 4 shows the sequence of cell activation on delivery of Wnts to the bath as a 2 µl bolus. As indicated by co-release with Alexa647, the cell response was a small reduction in Ca^{2+}_i as soon as the Wnt reached the cell (label 1, Figure 4A). This was followed by a rise in Ca^{2+}_i, after a delay of ~100s and coincided with a large increase in outward membrane current (label2). From the I=0 crossing of the current voltage curve the instantaneous membrane potential was determined. This potential will be referred to as the zero crossing potential, ZCP. In this case, the ZCP hyperpolarized, indicating that a K^+ current (i.e. K(Ca)) was activated.

At least two currents can be activated by Wnts. As well as a current attributed to K(Ca), (Figure 4A, label 2), a prolonged elevation of Ca^{2+}_i often coincided in a further current activation, sometimes in a stepwise fashion (e.g. at label 3, Figure 4A). Such current reversed near 0 mV. This could most easily be isolated if Cs^+ was included in the recording pipette to block K(Ca) (Figure 4C). The current-voltage curve (I-V) of such a Cs-insensitive current reversed near 0 mV. When such responses occurred, cells did not recover to a stable baseline.

There was no clear evidence for a voltage-gated Ca^{2+} entry into PC3 cells in the experimental conditions here despite earlier reports (Taylor *et al.*, 2008). However, a rise of Ca^{2+} was measured when cells were hyperpolarized (Figure 4D). Inclusion of 10 µM CID 755673 in the pipette, a known protein kinase D (PKD) inhibitor and cancer cell proliferation inhibitor (Sharlow *et al.*, 2008), had no effect on the Wnt responses (n=3 cells). This is consistent with the proposal that early Wnt events are not primarily acting via a conventional G protein mechanism but suggests that control of Ca^{2+}_i is transduced through the membrane by another mechanism.

Multi-well medium throughput determination of Wnt ligand action

Figure 5 near here

The membrane potential changes in PC3 cells showed a degree of variability both in amplitude and time course. To obtain precise control of steady state Wnt application and an estimate of the population behaviour, we employed a QPatch multi-well medium-throughput system with microfluidic control of the ligand delivery to measure up to 48 responses simultaneously (Figure 5). Under voltage clamp, ramps from (-120 to +120 mV) delivered every 3s showed pronounced outward current rectification at positive potentials. As with single cell recording there was a small outward holding current when the cells were held at -10 mV. Likewise, an estimate of the membrane potential was obtained from the I=0 crossing point of the ramped current. Measured in this way the ZCP was -21.1 ± 2.3 mV for Wnt5A.

PC3 cells also showed comparable membrane area to those reported using single cell recordings cultured on glass coverslips. The cell capacitance of cells recorded in the Q-Patch

system was 27.8 ± 1.4 pF (n=37) which compared with 31.2 ± 4.0 pF in a sample of n=12 single cell recordings made in whole cell tight seal mode.

The outward current at the +100 mV point of the ramp was used as a measure of Wnt activation. All three Wnts (5A, 9B and 10B) augmented this current (Figures 5A-C). The current can be identified as the progressive activation of a K^+ current. The half activation time of these currents was ~30 s for applied 3.5 nM Wnt5A, 9B and 10B. Such slow development of current in conjunction with the data presented in Figure 1, is consistent with the hypothesis that the prime source of Ca^{2+}_i was derived from intracellular stores rather than from entry from the extracellular solution.

I-V curves and the ZCP were also used to estimate the effects of Wnts on membrane potential from the ZCP. Figure 5 shows that Wnt5A, 9B and 10B (at 3.5 nM) hyperpolarized the cells. There was some variability in ZCPs, but these varied between cells in the range range -5 to -55 mV.

Microfluidic solution control in the Q-Patch showed that Wnt concentrations even at 2 nM elicited a response (Figure 5C). It should be noted at these lowest concentrations the currents built up slowly and would have been difficult to observe in single cell experiments. Although an outward K(Ca) current accounts for the resting current and change in the I-V curve, Q-Patch experiments sometimes showed a small dip of outward current occurring ~10s after the start of the Wnt application. Consistent with Ca^{2+} imaging (Figures 2 & 4), we suggest that this dip, as with single cells, was a result of deactivation of a standing K(Ca) at the holding potential of -10 mV.

Figure 6 near here

We also repeated the experiment (Figure 4C) of including Cs^+ in the pipette to block K(Ca). Figure 6 shows that no significant outward currents were produced by 3.5 nM Wnt5A (n=31) or Wnt9B (n=19, data not shown). The I-V relationship indicated a small reduction of the current at +100 mV although statistically not significant in this system. Together, results strongly suggest that K(Ca) is activated by internal Ca^{2+} release.

Current oscillations in PC3 cells in single cell patch clamp mode.

Figure 7 near here

Exposure to any of the Wnt ligands (5A, 9B and 10B) initiated low frequency oscillations in membrane current (Figure 7A-C) when the cell was held at 0 mV. The period determined from the first three peaks ranged from 15-30s for all Wnts (Figure 7D). Such oscillations are found in the control of Ca^{2+} store mechanisms in numerous systems (see Discussion). In a small number of cells the membrane potential and Ca^{2+}_i was measured together with Ca^{2+}_i (Figure 7E). The simultaneous Ca^{2+}_i levels fluctuated in antiphase to the membrane potential and strongly suggested that the Ca^{2+}_i fluctuations were driving the endogenous K(Ca) currents.

We conclude that Wnts control a pathway linked to internal Ca^{2+}_i stores and, as result, activated K(Ca) current. In addition, a small standing non-specific cation conductance pathway, responsible for a 'leak', offers an influx route for Ca^{2+} even in the absence of voltage gated Ca^{2+} channels. This could be a mechanism for further additional modulation Ca^{2+}_i homeostasis.

Targets for the early action of Wnt ligands

Figure 8 near here

The short latency of the responses (Figure 1) suggests that one early target might be an ion channel. In PC3 cells such a candidate is TRPM8 (Valero *et al.*, 2012; Asuthkar *et al.*, 2015b). To investigate this possibility the TRPM8 agonist, icilin (10 µM) was applied to the bath as a bolus. Icilin activated a small inward current (Figure 8 A,B) with a latency comparable to that found in Wnt experiments above. Although an order of magnitude smaller than the outward current, the induced outwardly rectifying current reversed at +15 mV consistent with the presence of TRPM8 (Andersson *et al.*, 2004). In support for this proposal, 100µM menthol, also a known agonist of TRPM8, close applied to PC3 cells generated a small depolarization. This depolarization was followed by a hyperpolarization which on, subsequent applications showed progressive reduction (Figure 8C). This would be expected if the activated Ca^{2+} stores were being progressively depleted.

We also found that, when present in the bath, 10 µM BCTC, a specific TRPM8 inhibitor (Madrid *et al.*, 2006), substantially reduced the response to Wnt5A and inhibited long lasting membrane oscillations and increased the latency of Wnt response (Figure 8D). The data, together with the action of the agonists menthol and icilin, indicate that TRPM8 is likely to be an early target that triggers store release of Ca^{2+} in these cells.

Discussion

We propose that Wnts can significantly increase K^+ permeability in a variety of mammalian cells lines, hyperpolarizing the cell and accelerating Ca^{2+}entry even in the absence of voltage-gated Ca^{2+} channels. Such an amplification mechanism would enhance Wnt as a trigger for signaling and subsequent translocation of its two key intracellular transducers, namely, Ca^{2+}_i and the transcription factor co-activator ß-catenin to the nucleus.

Little information exists on binding kinetics of Wnt ligands to their known receptors or the selectivity between different Wnt ligands and FZDs. By using bio-layer interferometry, it has been shown that the dissociation constants (K_D) for Wnts to FZD/CRD-Fc are in the range of 10-400 nM (Dijksterhuis *et al.*, 2015). These observations, albeit using a chemical approach, indicate that the time scale of Wnt ligand binding to the receptor is slow, e.g. k_{on} for Wnt3A and 5A ranges are between 2-3 $M^{-1}s^{-1}$ x10^4. Our results as in Figure 2 show that the first detectable interactions with Wnt could be measured within 100 ms in whole cells. The interactions with FZD receptor, and subsequent phosphorylation of LRP6 co-receptors are therefore likely to occur subsequent to the early interaction of Wnts with any ion channel targets.

The BKα subunit of the K(Ca) channel has been described using both molecular and functional assays in prostate cancer cell lines (Laniado *et al.*, 2001; Yan & Aldrich, 2010). The voltage activation of the α-subunit of the BK channel, the main K^+ permeation pathway in PC3 cells, paradoxically, lies well-positive to the observed cell resting potential of these cells (Yan & Aldrich, 2010) and thus it is the rise in Ca^{2+} that leads to opening of the identified BKα channel or secondary population of K(Ca) (e.g. KCNN4) channels (Lallet-Daher *et al.*, 2009). The low resting conductance in the PC3 cell line (6 nS) suggests that only a small

number of open K^+ channels would be sufficient to hyperpolarize the cell. Such small control currents could easily be overlooked in most leak-subtracted whole cell recordings (Laniado *et al.*, 2001; Yan & Aldrich, 2010) where the maximum activated currents (at +100 mV) can exceed 5 nA. The depolarized resting potential of such cells (Pardo & Stuhmer, 2014) shows that control of Ca^{2+}_i is independent of any voltage gated Ca^{2+}channel in the membrane, even though such mechanisms have been invoked in other cancer cells (Cruz-Cruz *et al.*, 2005). We thus predict that lowering extracellular K^+ might enhance the potency of Wnt signaling by inducing Ca^{2+}_i release and β-catenin translocation to the cell nucleus.

Figure 9 near here

A simplified model of the early events in Wnt signaling is given in Figure 9. The first event is a cell depolarization. We hypothesise that this occurs by activation of a small number of cation selective channels, with TRPM8 as a prime candidate. The PC3 cell line and other cancer cells, express several TRP channels (PCR data not shown) and, most prominently, TRPM4 and TRPM8 (Andersson *et al.*, 2004; Van Haute *et al.*, 2010; Valero *et al.*, 2012). We suggest that, like testosterone (Asuthkar *et al.*, 2015a), Wnts can have direct effect on TRP membrane channels. Both TRPM4 and TRPM8 are cation permeable, but TRPM8 in particular would be a favoured Ca^{2+} permeation route making it a plausible initial target for Wnt ligands (Zholos, 2010). The data do not reveal any entry of Ca^{2+} at this early first phase. It still remains possible however that Wnts may also activate a pathway in parallel which leads to store release and elevation of Ca^{2+}_i although on a slower time scale. An initial reduction in Ca^{2+}_i followed by a secondary Ca^{2+} release results in a buildup of Ca^{2+} near the membrane and activates K(Ca) channels to cause a hyperpolarization of the cell in response to Wnt signal activation. This model incorporates (although not shown in Figure 9 for clarity) established Wnt signaling events, i.e. Wnt binding to its receptors and co-receptors and the actions of downstream transducers such as Ca^{2+}_i release and β-catenin stabilization and translocation into the nucleus (Thastrup *et al.*, 1989; Contreras *et al.*, 2010; Thrasivoulou *et al.*, 2013).

The initial depolarization

The short-lasting depolarization preceding the cell hyperpolarization could be explained by activation of a cation selective channel. Were this channel also Ca^{2+} permeable, it might be

thought that the Ca^{2+} entering the cell would activate K(Ca) and lead to a Ca^{2+} induced release of Ca^{2+} (CICR) (Petrou *et al.*, 2017). However Figure 1D shows that cells respond even in the absence of external Ca^{2+} (see also (Thrasivoulou *et al.*, 2013)) and this proposal must therefore be modified.

The initial fall in Ca^{2+}_i (apparent in Figures 2, 4) could be due to the activation of a Ca^{2+}_i buffering mechanism. It could also arise when both monovalent and divalent cations share the same pore, as might be the case for TRPM8, as the driving force is reduced and equilibrium Ca^{2+}_i falls. Appendix A1 gives an argument based on the Goldman-Hodgkin-Katz equation for this conclusion and shows that the apparent permeability of such a pore for Ca^{2+} *decreases* as the cell depolarizes (Lewis, 1979). The mechanism is similar to that in olfactory ensheathing cells which likewise exhibit a Ca^{2+}_i fall when depolarized (Hayat *et al.*, 2003). Such a cytoplasmic Ca^{2+}_i reduction could then initiate further release from the cell's internal stores leading to the Ca^{2+}_i rise observed.

We have previously shown (Thrasivoulou *et al.*, 2013) that Wnt induced Ca^{2+}_i release is inhibited by SERCA inhibitors such as thapsigargin (Thastrup *et al.*, 1989), although the role of other organelles involved in Ca^{2+} storage and release e.g. mitochondria, Golgi apparatus, lysomes (Contreras *et al.*, 2010) remains to be explored. Thus, we cannot rule out activation of other triggering systems for Ca^{2+}_i elevation operating in parallel. However, such systems would need to operate on a sub-second time scale and might well imply a heterogeneous distribution of 'hotspots' (data not shown) where the Ca^{2+}_i levels are elevated, possibly associated with release from the endoplasmic reticular stores. Such heterogeneities can in principle be detected with high spatial resolution microscopy.

Oscillatory responses in PC3 cells

Slow oscillatory Ca^{2+} activated currents have been reported in a variety of tissues including mammary cells (Enomoto *et al.*, 1991), oocytes (Miledi *et al.*, 1987) and smooth muscle (Kajioka *et al.*, 2004). A proportion (approximately 20%) of imaged cells also showed oscillations in Ca^{2+}_i (Thrasivoulou *et al.*, 2013). The observed oscillations in the present study could arise either through intrinsic negative feedback mechanisms in the Wnt signaling pathway or more probably through Ca^{2+} control of the Ca^{2+} entry pathway itself. It

is known for example, that Orai1, a good candidate for the cation entry permeability, is itself inhibited by Ca^{2+}_i (Scrimgeour *et al.*, 2009). A variety of intracellular Ca^{2+} signaling models implicating the internal stores predict oscillatory behaviour with the appropriate time course (Schuster *et al.*, 2002). The oscillations observed here in both current and potential (Figure 7) are therefore compatible with a feedback involving store release and refilling with Ca^{2+}.

Long latency events in activation of a cation current

An early reduction in Ca^{2+}_i, particularly if in close association with the internal stores, would be expected to act as a trigger for store release and then would be followed by store operated Ca^{2+} entry (SOCE) (Lallet-Daher *et al.*, 2009). The long latency current activated by an elevated Ca^{2+}_i resemble many characteristics of the SOCE channels Orai1 and Orai3 (Vanden Abeele *et al.*, 2003). Such cation currents suggest the presence of underlying Orai1 or Orai3 channels. First, these channels are both Ca^{2+} and monovalent cation permeable (Scrimgeour *et al.*, 2009); second, they have been described in many cancer cell lines (Prakriya & Lewis, 2015; Stanisz *et al.*, 2016); third, the Orai1-Stim complex has been shown to be over-expressed in another cancer cell line under transcriptional regulation of Wnt5A signal (Hooper *et al.*, 2015; Stanisz *et al.*, 2016); and fourth the STIM-Orai complex is activated by Ca^{2+} induced store depletion.

In summary, we have shown that Wnts act as ligands to activate K^+ and non-selective channels in mammalian cell membranes at nanomolar concentrations. We have shown that Wnt ligand interaction at the cell membrane initiates a sequence where Ca^{2+}_i increases, opening K(Ca) channels and then activation of SOCE channels (but only if the rise of Ca^{2+}_i is sufficient to deplete stores and producing an STIM/Orai activation). The possibility of intermediate involvement of e.g. inositol 1,4,5-trisphosphate (IP3) and ryanodine receptors is not excluded. Our observations regarding the early events of Wnt interaction at the cell membrane provide rapid biological assay to investigate Wnt activity. These measures, in conjunction with the use of medium-throughput electrophysiological analysis using a QPatch system, provide a novel tool for mechanistic understanding or screening of small molecule Wnt modulators that may act at the cell membrane to inhibit or activate the

downstream signaling.

There are significant implications for the downstream actions for the Wnt signaling pathway which is critical during development and in proliferative diseases such as cancer. Thus, in addition to being a quick, quantitative, readout of Wnt activity, an understanding of the Wnt control of cell membrane potential may facilitate development of therapies. The data open the possibility that the cell membrane potential may control the nature of Wnt binding at the cell surface and the temporal coding of an intracellular signal transduction including ß-catenin transcription to the nucleus. It is possible that ligands for signal transduction pathways, other than the Wnt network, may also utilize electrical mechanisms for temporal and feedback controls of the signaling.

Acknowledgements

The project was conceived by AA. JFA, HO, NMS and AA carried out the experiments. HO, CT, JFA and AA analyzed the data. JFA and AA wrote the manuscript. The work was funded by a grant to AA from the Prostate Cancer Research charity (registered UK charity no. 1156027). We thank John R W Masters for cell lines used in this study, support and discussions. We are also grateful to Tony Davies for support and discussions and Jane Pendjiky and Callum Arthurs for help with figures.

Figure legends:

Figure 1. Wnts activate membrane potential changes

A) Characteristic morphology of PC3 cell imaged while applying Wnt and solutions from a closely opposed pipette. Cells were selected to be relatively isolated. Scale, 20 µm.

B) Distribution of resting potentials determined under current clamp of sample, -23.8 ± 2.54 mV (n=59);

C) Wnt 9B hyperpolarization of a cell upon a 2 s pressure pulse from the pipette. The trace shows the onset timing of the application. The puff pipette contained 120 nM Wnt 9B. RP = -7 mV.

D) Wnt 5A hyperpolarization of a cell. The depolarization preceded the hyperpolarization, as soon as the Wnt reached the cell. Puff pipette contained 35 nM Wnt 5A. Wnt application monitored by 633 nm excitation of Alexa647 in the puff pipette. The signal level was kept low to ensure linearity for measurement but calibrated against the maximum fluorescence.

E) Wnt ligands (5A and 9B) caused a biphasic change in membrane potential, (Vm). The box plots show the distribution of Vm depolarization and hyperpolarization in response to Wnt ligands (n=9-19: The depolarization amplitude was 4.6 ± 1.6 mV (n=13) and 5.4 ± 1.4 mV (n=13) for Wnt 5A and Wnt 9B respectively and a hyperpolarization of -12.7 ± 2.5 mV (n=19) and -11.2 ± 4.6 mV (n=9), respectively).

F) External Ca^{2+} was not required for hyperpolarization. Membrane potential response induced by Wnt 5A in PC3 cells was measured with low external Ca^{2+} (with the estimated extracellular Ca^{2+} at < 1 µM) by introduction of 5 mM EGTA into the nominally 0 Ca^{2+} bath solution. Wnt was delivered as a 2 µL bolus, resulting in a slower onset of the depolarization over 50-100 s as the Wnt concentration increased (see Methods). Representative of n=4 experiments.

Figure 2. Rapid responses to Wnt application

A) Line scan and profile of a cell loaded with the 200 µM OGB-5N, showing the scanned profile of the cell. Arrow indicates the direction of signal increase. B) x-t display of intracellular OGB-5N and Wnt (Alexa647) recorded on separate channels, 65 µm line scanned at 125 Hz. C) Simultaneous membrane potential (mV, I=0 current clamp) and from

the x-t display, D) OGB-5N Ca^{2+} fluorescence and E) Alexa647 signals for the dye delivery. The estimated maximum Wnt concentration was 44 nM. Two time scales are displayed to show the early signal elicited within 100 ms and a later hyperpolarization. The Wnt application hyperpolarized the cell (from RP = -43 mV), but also produced an early small depolarization.

Figure 3. Wnt responses in cancer cells lines

A-C) PC3 cells showed an I-V with outward rectification. When raw data were plotted (closed circles), the outward rectification is often accompanied by a small leak current. The net effect is a zero current potential (ZCP) near -10 mV. A) representative current traces elicited in PC3 cells by (B) command voltage steps. C) I-V curves from raw (filled symbol) and leak subtracted (hollow symbol) data.

D-O) Wnts increase currents in PC3, MCF7 and LnCAP cell lines (n=5-40). The I-V relations for each cell before (hollow symbols) and during (filled symbols) show that at the peak of the Wnt response, the ZCP remained near 0 mV, indicating the activation of primarily a cation-selective current. The intercept of the PC3 I-V curve with the I=0 axis exhibited a 33 mV hyperpolarizing shift (from -15 to – 48 mV shown as an indicator bar on the abscissa, G). (D, H and L), current traces without and (E,I and M) ~200 s after Wnt added as a bolus to the bath. (B,F,J and N), command steps, 100 ms or 50 ms.

Figure 4. Long latency responses to Wnt

A) Representative application of Wnt9B in whole cell recording mode (holding potential = -25 mV). Wnt applied as a bolus to the bath at t=0, monitored by extracellular Alexa647 dye. OGB-5N (200 µM) in recording pipette. A delay of 20s, partially attributable to diffusion, occurred before the Wnt ligand reached the cell. The initial response was a reduction of Ca^{2+} (phase 1) with a decrease in the holding current, followed by (phase 2) an increase in current, attributable to K(Ca) activation. In some cells, there were marked inward current steps (phase 3), especially when held at negative potentials as here. Similar results were observed for all cells, with variable delays depending on the dynamics of solution mixing in the bath. Ca^{2+} fluorescence increased after ~150s and was associated with increased cell input conductance.

B) Distribution of outward holding current, i_{hold} in a sample of cells held at 0 mV. I_{hold} = 38.4 ± 2.4 pA (n=40). Distribution of additional outward current at 200 s after cells activated by Wnt5A (0.329 ± 0.095 nA, n=22) and by Wnt9B (0.458 ± 0.172 nA, n=10).

C) K(Ca) current blocked with 140 mM Cs^+ in the pipette. 3 min after break in, ramps showed reduced outward rectification. With a delay, Wnt9B activated a large current reversing at near 0 mV when a bolus was applied.

D) Membrane polarization altered intracellular Ca^{2+} with -50 mV hyper- or +50 mV depolarizing steps, increasing or decreasing respectively the intracellular fluorescence. The outward current rebound on return to 0 mV from -50 mV was consistent with the activation of a K(Ca) current on hyperpolarization.

Figure 5. Wnts determine currents in a medium throughput QPatch system

A) Wnt 5A, 9B and 10B activated currents (panel of black traces) in PC3 cells were measured concurrently using a QPatch system (Sophion) in 3x16 well plates. Gray bar indicates the period (300s) between which the cells were exposed to Wnts. The cells were held at -10 mV and ramped at 0.5 mV/ms from -120 to +120 mV every 3 s. The panels show representative traces of the currents measured at +100 mV from a selection of three distinct experiments.

B) The average currents (measured at +100 mV shown for Wnt5A, Wnt9B and Wnt10B (n=9-18 cells). All doses, 3.5 nM. Data from a single 48 well experimental run. The S.E.M. is shown only at 15 s points. The calculated zero current potential (ZCP) in mV calculated from the I-V intercept is shown in below each current trace. Only cells where the input conductance <10 nS were analyzed. In the QPatch system, complete solution changes could be made within 500 ms.

C) Wnts act at nanomolar concentrations elicited responses. Currents at +100 mV of a ramp when different Wnt 5A concentrations were applied in QPatch system (n= 4-6 cells for each concentration). In each case the Wnt application hyperpolarized the cell when computed from the ZCP (not shown).

Figure 6. Wnt currents are blocked by Cs in a medium throughput QPatch system

A) Effect of internal 120 mM Cs^+ on the Wnt5A (3.5 nM) induced currents at +100 mV. Results show that the outward rectification and Wnt response was blocked (n=31). A small drift has been removed from the data. Comparable absence of response for Wnt 9B (n=19)

was also observed.

B) Average IVs (n=31) comparing ramps just before and at 60s after the application of 3.5 nM Wnt5A. The outward rectification due to K(Ca) has been significantly reduced as a result of the Cs^{+}_{i}, revealing a small current which reversed near 0 mV. The slope conductance at 0 mV was reduced from 8.6 nS to 7.7 nS by Wnt5A.

Figure 7. Oscillatory responses to Wnts in single cells

A-C) Cells showed an oscillatory current in response to Wnts 5A, 9B and 10B tested. 2 µl boli of each Wnt applied to the bath to reach a final concentration of 4 nM. Variable diffusion delays between the Wnt application and oscillatory responses were due to differing geometries of bolus application from experiment to experiment. Holding potential, 0 mV.

D) Interspike period of current oscillations in PC3 cells to Wnts 5A (n=15), Wnt 9B (n=4), Wnt 10B (n=4).

E) Membrane potential oscillations produced by Wnt 9B after a bolus application. Simultaneous Ca^{2+}_{i} records (gray trace) showed that the oscillation peaked in antiphase to membrane potential (black trace), consistent with an increase of Ca^{2+}_{i} causing cell hyperpolarization.

Figure 8. Activation of PC3 cells by TRPM8 agonists

A) Icilin (10 µM) applied as a bolus to the bath at stimulus marker (arrow) produced an inward current in voltage clamped PC3 cells. Holding potential, 0 mV. The currents generated by a series of command steps for an I-V curve, delivered every 30 s, have been suppressed for clarity.

B) I-V curves for the currents elicited just before (hollow circles) and at 150 s after icilin (filled circles) application, showing growth of both inward and outward currents, both reversing near 0 mV. Icilin activated an outwardly rectifying current reversing at +15 mV.

C) Membrane potential changes elicited by 100 µM menthol puff applied to the cell in 8.5 s pulses every 90 s, labelled in sequence. Menthol elicited a depolarization, followed by a hyperpolarization which progressively diminished with successive applications (labelled 1-3), showing run-down of the response.

D) Wnt 5A (3.5 nM) induced currents measured in the presence (black) or absence (grey) of BCTC (10 µM), V_h = -10 mV. There was a increase in the latency of Wnt induced current in the presence of BCTC.

Figure 9. A model for early events in Wnt signal activation at the cell membrane

Wnt activates a trigger mechanism at the cell membrane to initiate a signal cascade (numbered 1-7). A small standing K^+ permeability coupled with permeability to cations ensures that the cells are only slightly hyperpolarized. Our model consists of the following steps: (1) Wnt ligand binds to its known receptors FZD/LRP6 and TRPM8 (time scale <0.1s) and depolarization of the cell, resulting in (2) $Ca^{2+}{}_i$ reduction (see Appendix A1, depleting the endoplasmic reticulum (ER) and/or the mitochondrial stores), (3) triggering a Ca^{2+} release and (4) buildup (time scale ~ 10 s) of Ca^{2+} near the membrane; (5) activation of K(Ca) channels then hyperpolarizes the cell membrane. On a time scale of ~ 100 s, the Ca^{2+} depletion from the ER stores leads to (6) opening of the SOCE channels (STIM/Orai1+3) to replenish ER Ca^{2+} stores which produces a large cation current repolarizing the cell. Subsequently, (7) $Ca^{2+}{}_i$ enters the nucleus where it is likely to facilitate the entry of ß-catenin (a transcription factor co-activator and a key intracellular transducer of Wnt signaling, omitted from this diagram for clarity but described elsewhere (Thrasivoulou *et al.*, 2013)). A contribution from classical activation of a FZD/LRP6 pathway is not ruled out and the role of other intermediary Ca^{2+} release mechanisms (e.g. IP3 and ryanodine receptors) is not excluded. For clarity, only events related to Wnt induced Ca^{2+} release are shown.

Appendix A1

Dependence of Ca^{2+}_i on membrane potential for a monovalent and divalent permeable channel.

According to Lewis (Lewis, 1979), the Goldman Hodgkin Katz equation describing the equilibrium potential V_o modified to include the effect of the divalent cation Ca^{2+} permeating through a single pore is

$$V_0 = \frac{RT}{F} \ln \frac{[\mathrm{Na}]_o + \frac{P_K}{P_{Na}}[\mathrm{K}]_o + 4\frac{P'_{Ca}}{P_{Na}}[\mathrm{Ca}]_o}{[\mathrm{Na}]_i + \frac{P_K}{P_{Na}}[\mathrm{K}]_i + 4\frac{P'_{Ca}}{P_{Na}}[\mathrm{Ca}]_i e^{FV_0/RT}}.$$

where

$$P'_{Ca} = \frac{P_{Ca}}{1 + e^{FV/RT}}.$$

and P_{Na} and P_K have the standard meanings. Thus the effective Ca^{2+} permeability is voltage sensitive, decreasing as the cell depolarizes. Accordingly, if K and Na have equal permeabilities though the channel, and the total concentration, X, of monovalent cations is the same on both sides of the membrane,

$$Na_o + K_o = Na_i + K_i = X$$

and assuming equal permeability for the Na and K ions, (i.e. $P_{Na}=P_K=P_X$), and an externally fixed Ca^{2+} (Ca_o) concentration, the internal Ca^{2+} (Ca_i) becomes a function of V and P_{Ca}/P_X only. A little algebra then shows

$$Ca_i = Ca_0 \exp(-2\ FV/RT) - (P_X / 4\ P_{Ca})\ .\ X.\ (1-\exp(-2FV/RT))$$

Near V=0, as in this case, the <u>equilibrium</u> Ca_i is a monotonically decreasing function of membrane potential, V. Thus, either by direct simulation or analytically, we see that as V increases then equilibrium levels of Ca_i falls. Even for relatively low calcium permeabilities, P_{Ca}, the effect can be quite large since, because of charge balance, Ca^{2+} is constrained to leave the cell.

References

Andersson DA, Chase HW & Bevan S. (2004). TRPM8 activation by menthol, icilin, and cold is differentially modulated by intracellular pH. *J Neurosci* **24,** 5364-5369.

Asuthkar S, Demirkhanyan L, Sun X, Elustondo PA, Krishnan V, Baskaran P, Velpula KK, Thyagarajan B, Pavlov EV & Zakharian E. (2015a). The TRPM8 protein is a testosterone receptor: II. Functional evidence for an ionotropic effect of testosterone on TRPM8. *J Biol Chem* **290,** 2670-2688.

Asuthkar S, Velpula KK, Elustondo PA, Demirkhanyan L & Zakharian E. (2015b). TRPM8 channel as a novel molecular target in androgen-regulated prostate cancer cells. *Oncotarget* **6,** 17221-17236.

Bilic J, Huang YL, Davidson G, Zimmermann T, Cruciat CM, Bienz M & Niehrs C. (2007). Wnt induces LRP6 signalosomes and promotes dishevelled-dependent LRP6 phosphorylation. *Science* **316,** 1619-1622.

Bourhis E, Tam C, Franke Y, Bazan JF, Ernst J, Hwang J, Costa M, Cochran AG & Hannoush RN. (2010). Reconstitution of a frizzled8.Wnt3a.LRP6 signaling complex reveals multiple Wnt and Dkk1 binding sites on LRP6. *J Biol Chem* **285,** 9172-9179.

Clevers H & Nusse R. (2012). Wnt/beta-catenin signaling and disease. *Cell* **149,** 1192-1205.

Contreras L, Drago I, Zampese E & Pozzan T. (2010). Mitochondria: the calcium connection. *Biochim Biophys Acta* **1797,** 607-618.

Cruz-Cruz R, Salgado A, Sanchez-Soto C, Vaca L & Hiriart M. (2005). Thapsigargin-sensitive cationic current leads to membrane depolarization, calcium entry, and insulin secretion in rat pancreatic beta-cells. *Am J Physiol Endocrinol Metab* **289,** E439-445.

Dijksterhuis JP, Baljinnyam B, Stanger K, Sercan HO, Ji Y, Andres O, Rubin JS, Hannoush RN & Schulte G. (2015). Systematic mapping of WNT-FZD protein interactions reveals functional selectivity by distinct WNT-FZD pairs. *J Biol Chem* **290,** 6789-6798.

Dijksterhuis JP, Petersen J & Schulte G. (2014). WNT/Frizzled signalling: receptor-ligand selectivity with focus on FZD-G protein signalling and its physiological relevance: IUPHAR Review 3. *Br J Pharmacol* **171,** 1195-1209.

Enomoto K, Furuya K, Maeno T, Edwards C & Oka T. (1991). Oscillating activity of a calcium-activated K+ channel in normal and cancerous mammary cells in culture. *J Membr Biol* **119,** 133-139.

Grundmann M & Kostenis E. (2017). Temporal Bias: Time-Encoded Dynamic GPCR Signaling. *Trends Pharmacol Sci* **38,** 1110-1124.

Hayat S, Wigley CB & Robbins J. (2003). Intracellular calcium handling in rat olfactory ensheathing cells and its role in axonal regeneration. *Mol Cell Neurosci* **22,** 259-270.

Hooper R, Zhang X, Webster M, Go C, Kedra J, Marchbank K, Gill DL, Weeraratna AT, Trebak M & Soboloff J. (2015). Novel Protein Kinase C-Mediated Control of Orai1 Function in Invasive Melanoma. *Mol Cell Biol* **35,** 2790-2798.

Kajioka S, Nakayama S, McCoy R, McMurray G, Abe K & Brading AF. (2004). Inward current oscillation underlying tonic contraction caused via ETA receptors in pig detrusor smooth muscle. *Am J Physiol Renal Physiol* **286,** F77-85.

Klaus A & Birchmeier W. (2008). Wnt signalling and its impact on development and cancer. *Nat Rev Cancer* **8,** 387-398.

Lallet-Daher H, Roudbaraki M, Bavencoffe A, Mariot P, Gackiere F, Bidaux G, Urbain R, Gosset P, Delcourt P, Fleurisse L, Slomianny C, Dewailly E, Mauroy B, Bonnal JL, Skryma R & Prevarskaya N. (2009). Intermediate-conductance Ca2+-activated K+ channels (IKCa1) regulate human prostate cancer cell proliferation through a close control of calcium entry. *Oncogene* **28,** 1792-1806.

Laniado ME, Fraser SP & Djamgoz MB. (2001). Voltage-gated K(+) channel activity in human prostate cancer cell lines of markedly different metastatic potential: distinguishing characteristics of PC-3 and LNCaP cells. *Prostate* **46,** 262-274.

Lewis CA. (1979). Ion-concentration dependence of the reversal potential and the single channel conductance of ion channels at the frog neuromuscular junction. *J Physiol* **286,** 417-445.

Madrid R, Donovan-Rodriguez T, Meseguer V, Acosta MC, Belmonte C & Viana F. (2006). Contribution of TRPM8 channels to cold transduction in primary sensory neurons and peripheral nerve terminals. *J Neurosci* **26,** 12512-12525.

Miledi R, Parker I & Sumikawa K. (1987). Oscillatory chloride current evoked by temperature jumps during muscarinic and serotonergic activation in Xenopus oocyte. *J Physiol* **383,** 213-229.

Narendra Talabattula VA, Morgan P, Frech MJ, Uhrmacher AM, Herchenroder O, Putzer BM, Rolfs A & Luo J. (2017). Non-canonical pathway induced by Wnt3a regulates beta-catenin via Pyk2 in differentiating human neural progenitor cells. *Biochem Biophys Res Commun* **491,** 40-46.

Noyer L, Grolez GP, Prevarskaya N, Gkika D & Lemonnier L. (2018). TRPM8 and prostate: a cold case? *Pflugers Arch* **470,** 1419-1429.

Nusse R. (2012). Wnt signaling. *Cold Spring Harb Perspect Biol* **4**.

Pardo LA & Stuhmer W. (2014). The roles of K(+) channels in cancer. *Nat Rev Cancer* **14,** 39-48.

Pastan IH & Willingham MC. (1981). Journey to the center of the cell: role of the receptosome. *Science* **214,** 504-509.

Petrou T, Olsen HL, Thrasivoulou C, Masters JR, Ashmore JF & Ahmed A. (2017). Intracellular Calcium Mobilization in Response to Ion Channel Regulators via a Calcium-Induced Calcium Release Mechanism. *J Pharmacol Exp Ther* **360,** 378-387.

Prakriya M & Lewis RS. (2015). Store-Operated Calcium Channels. *Physiol Rev* **95,** 1383-1436.

Schuster S, Marhl M & Hofer T. (2002). Modelling of simple and complex calcium oscillations. From single-cell responses to intercellular signalling. *Eur J Biochem* **269,** 1333-1355.

Schwarz-Romond T. (2012). Three decades of Wnt signalling. *EMBO J* **31,** 2664.

Scrimgeour N, Litjens T, Ma L, Barritt GJ & Rychkov GY. (2009). Properties of Orai1 mediated store-operated current depend on the expression levels of STIM1 and Orai1 proteins. *J Physiol* **587,** 2903-2918.

Sharlow ER, Giridhar KV, LaValle CR, Chen J, Leimgruber S, Barrett R, Bravo-Altamirano K, Wipf P, Lazo JS & Wang QJ. (2008). Potent and selective disruption of protein kinase D functionality by a benzoxoloazepinolone. *J Biol Chem* **283,** 33516-33526.

Sklar LA, Finney DA, Oades ZG, Jesaitis AJ, Painter RG & Cochrane CG. (1984). The dynamics of ligand-receptor interactions. Real-time analyses of association, dissociation, and internalization of an N-formyl peptide and its receptors on the human neutrophil. *J Biol Chem* **259,** 5661-5669.

Stanisz H, Vultur A, Herlyn M, Roesch A & Bogeski I. (2016). The role of Orai-STIM calcium channels in melanocytes and melanoma. *J Physiol* **594,** 2825-2835.

Taylor JT, Zeng XB, Pottle JE, Lee K, Wang AR, Yi SG, Scruggs JA, Sikka SS & Li M. (2008). Calcium signaling and T-type calcium channels in cancer cell cycling. *World J Gastroenterol* **14,** 4984-4991.

Thastrup O, Dawson AP, Scharff O, Foder B, Cullen PJ, Drobak BK, Bjerrum PJ, Christensen SB & Hanley MR. (1989). Thapsigargin, a novel molecular probe for studying intracellular calcium release and storage. *Agents Actions* **27,** 17-23.

Thrasivoulou C, Millar M & Ahmed A. (2013). Activation of intracellular calcium by multiple Wnt ligands and translocation of beta-catenin into the nucleus: a convergent model of Wnt/Ca2+ and Wnt/beta-catenin pathways. *J Biol Chem* **288,** 35651-35659.

Valero ML, Mello de Queiroz F, Stuhmer W, Viana F & Pardo LA. (2012). TRPM8 ion channels differentially modulate proliferation and cell cycle distribution of normal and cancer prostate cells. *PLoS One* **7,** e51825.

Van Haute C, De Ridder D & Nilius B. (2010). TRP channels in human prostate. *ScientificWorldJournal* **10,** 1597-1611.

Vanden Abeele F, Shuba Y, Roudbaraki M, Lemonnier L, Vanoverberghe K, Mariot P, Skryma R & Prevarskaya N. (2003). Store-operated Ca2+ channels in prostate cancer epithelial cells: function, regulation, and role in carcinogenesis. *Cell Calcium* **33,** 357-373.

Yan J & Aldrich RW. (2010). LRRC26 auxiliary protein allows BK channel activation at resting voltage without calcium. *Nature* **466,** 513-516.

Zeng X, Tamai K, Doble B, Li S, Huang H, Habas R, Okamura H, Woodgett J & He X. (2005). A dual-kinase mechanism for Wnt co-receptor phosphorylation and activation. *Nature* **438,** 873-877.

Zholos A. (2010). Pharmacology of transient receptor potential melastatin channels in the vasculature. *Br J Pharmacol* **159,** 1559-1571.

Figure 1

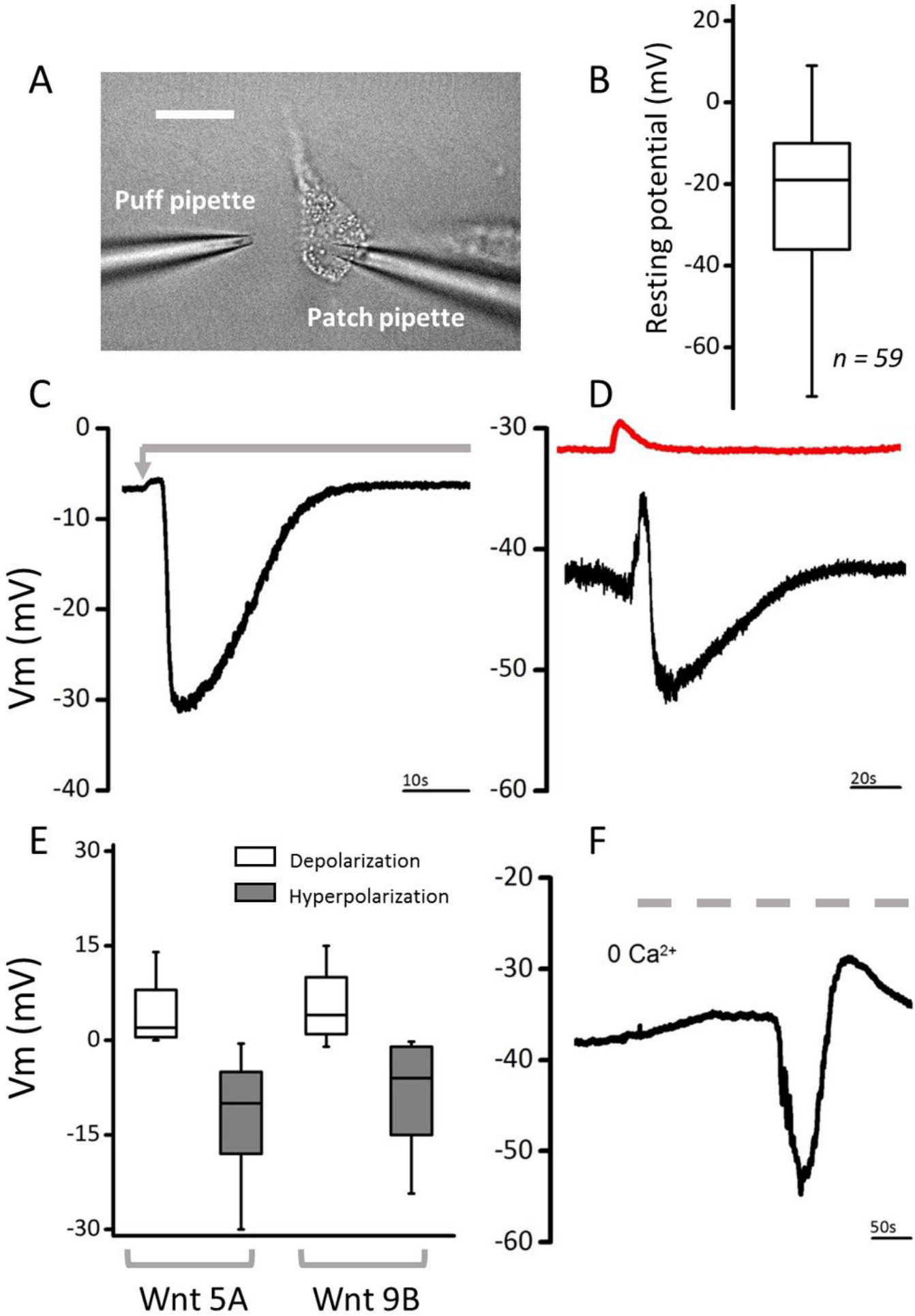
A
Puff pipette
Patch pipette
B
Resting potential (mV)
20
0
-20
-40
-60
n = 59
C
Vm (mV)
0
-10
-20
-30
-40
10s
D
-30
-40
-50
-60
20s
E
Depolarization
Hyperpolarization
Vm (mV)
30
15
0
-15
-30
Wnt 5A
Wnt 9B
F
0 Ca2+
-20
-30
-40
-50
-60
50s

Figure 2

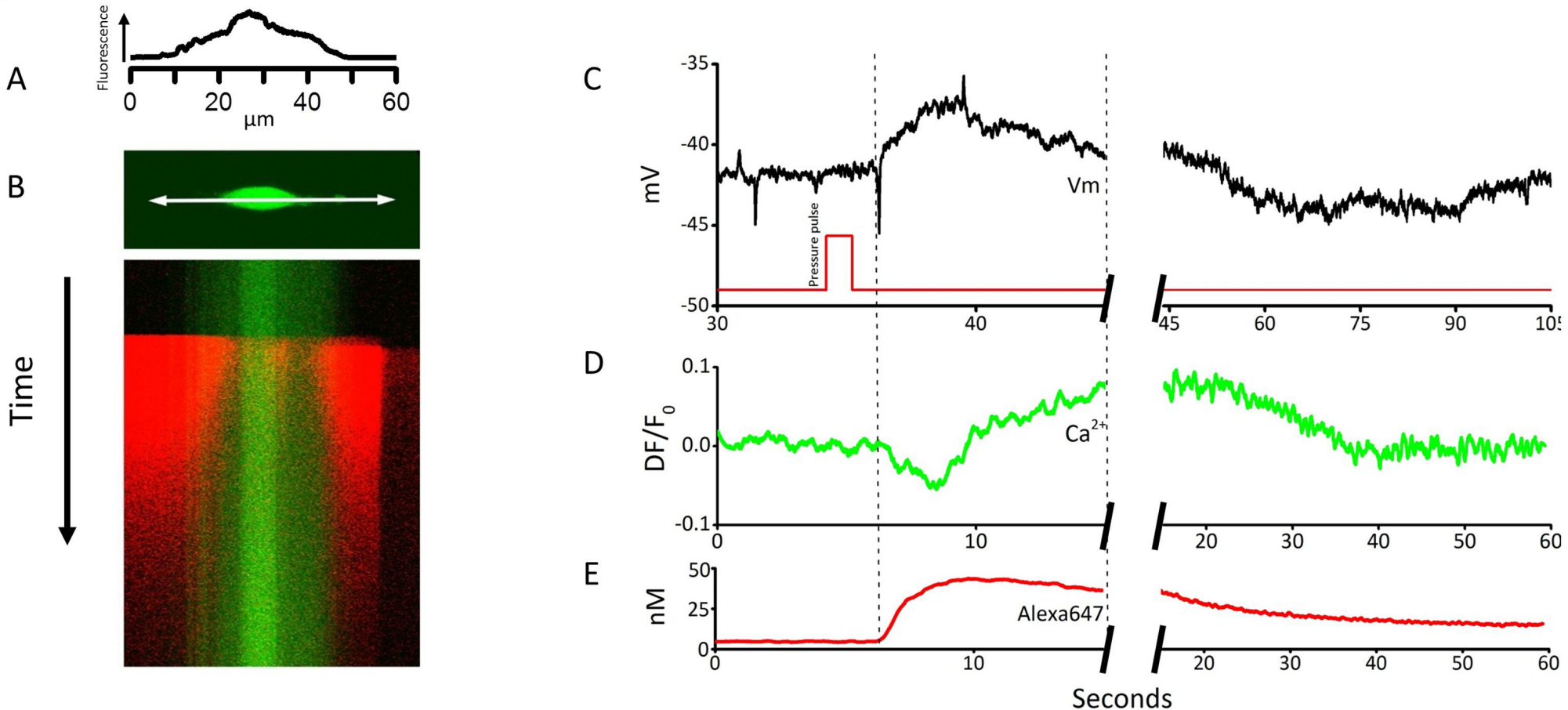
A
Fluorescence
0
20
40
60
µm
B
Time
C
mV
-35
-40
-45
-50
Vm
Pressure pulse
30
40
45
60
75
90
105
D
DF/F0
0.1
0.0
-0.1
Ca2+
0
10
20
30
40
50
60
E
nM
50
25
0
Alexa647
0
10
20
30
40
50
60
Seconds

Figure 3

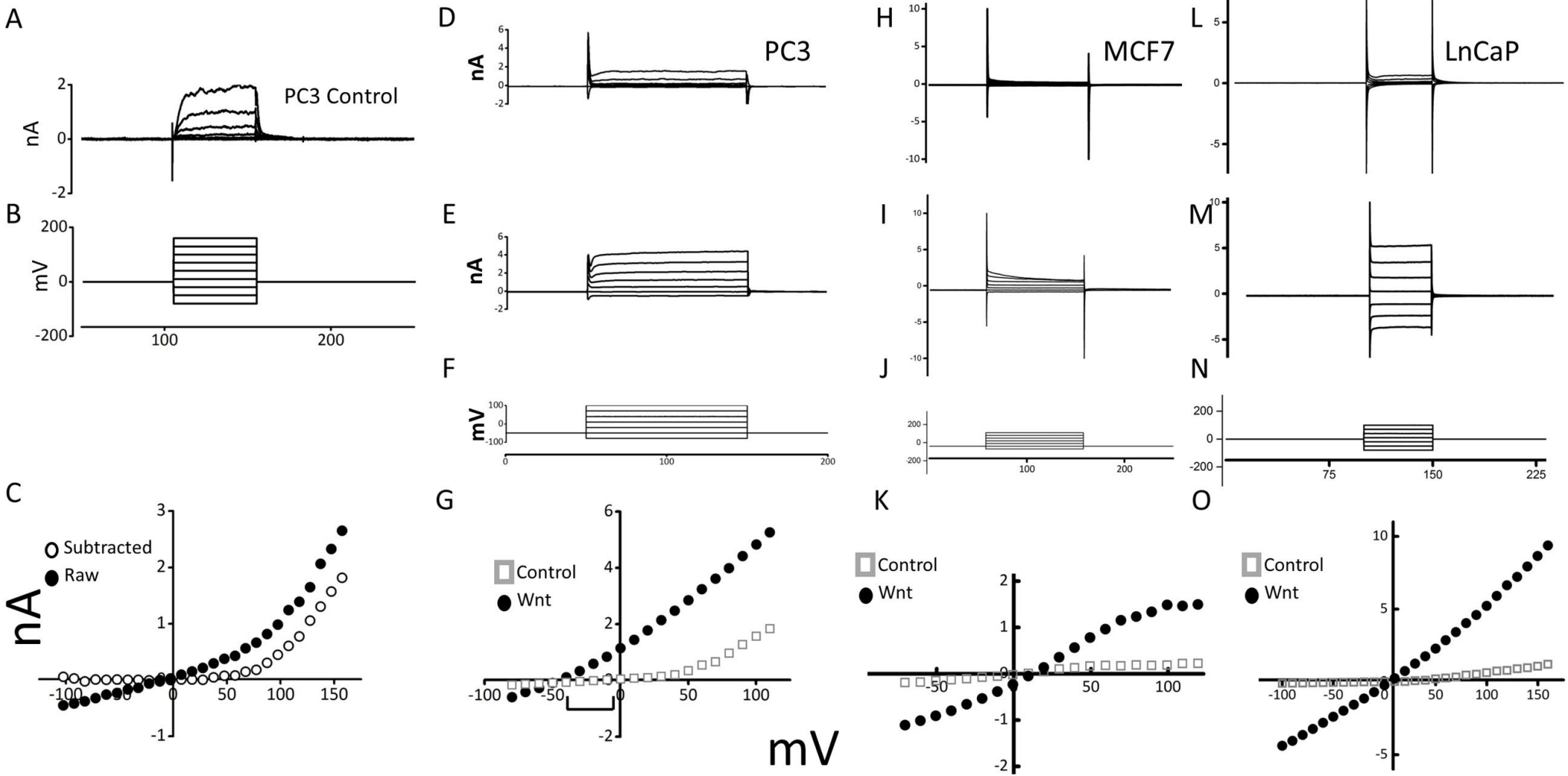
A
PC3 Control
nA
B
mV
C
Subtracted
Raw
nA
D
PC3
nA
E
nA
F
mV
H
MCF7
I
J
L
LnCaP
M
N
G
Control
Wnt
mV
K
Control
Wnt
O
Control
Wnt

Figure 4

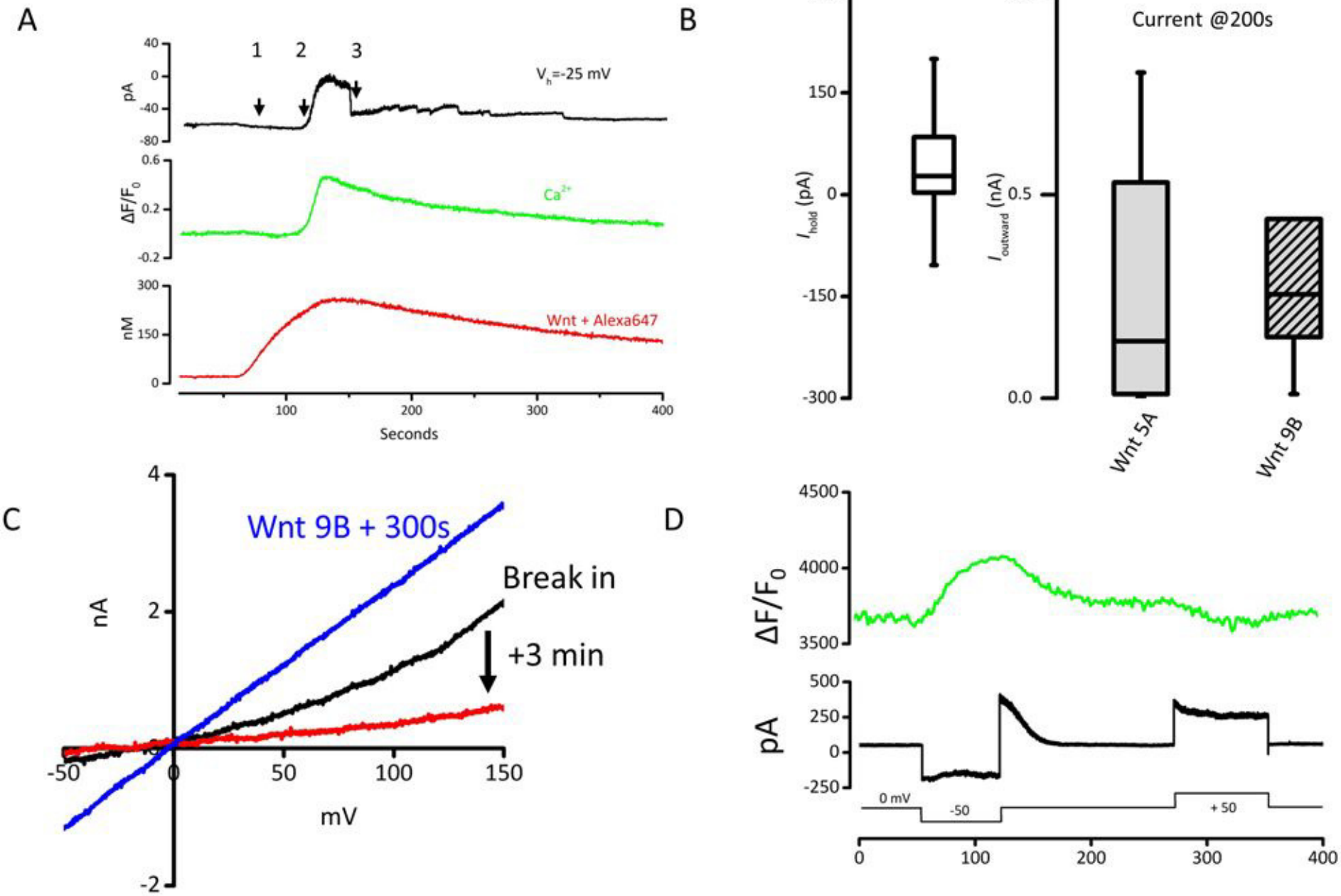
A
1
2
3
V_h=-25 mV
pA
$\Delta F/F_0$
Ca^{2+}
nM
Wnt + Alexa647
Seconds
B
Current @200s
I_{hold} (pA)
$I_{outward}$ (nA)
Wnt 5A
Wnt 9B
C
Wnt 9B + 300s
Break in
+3 min
nA
mV
D
$\Delta F/F_0$
pA
0 mV
-50
+ 50

Figure 5

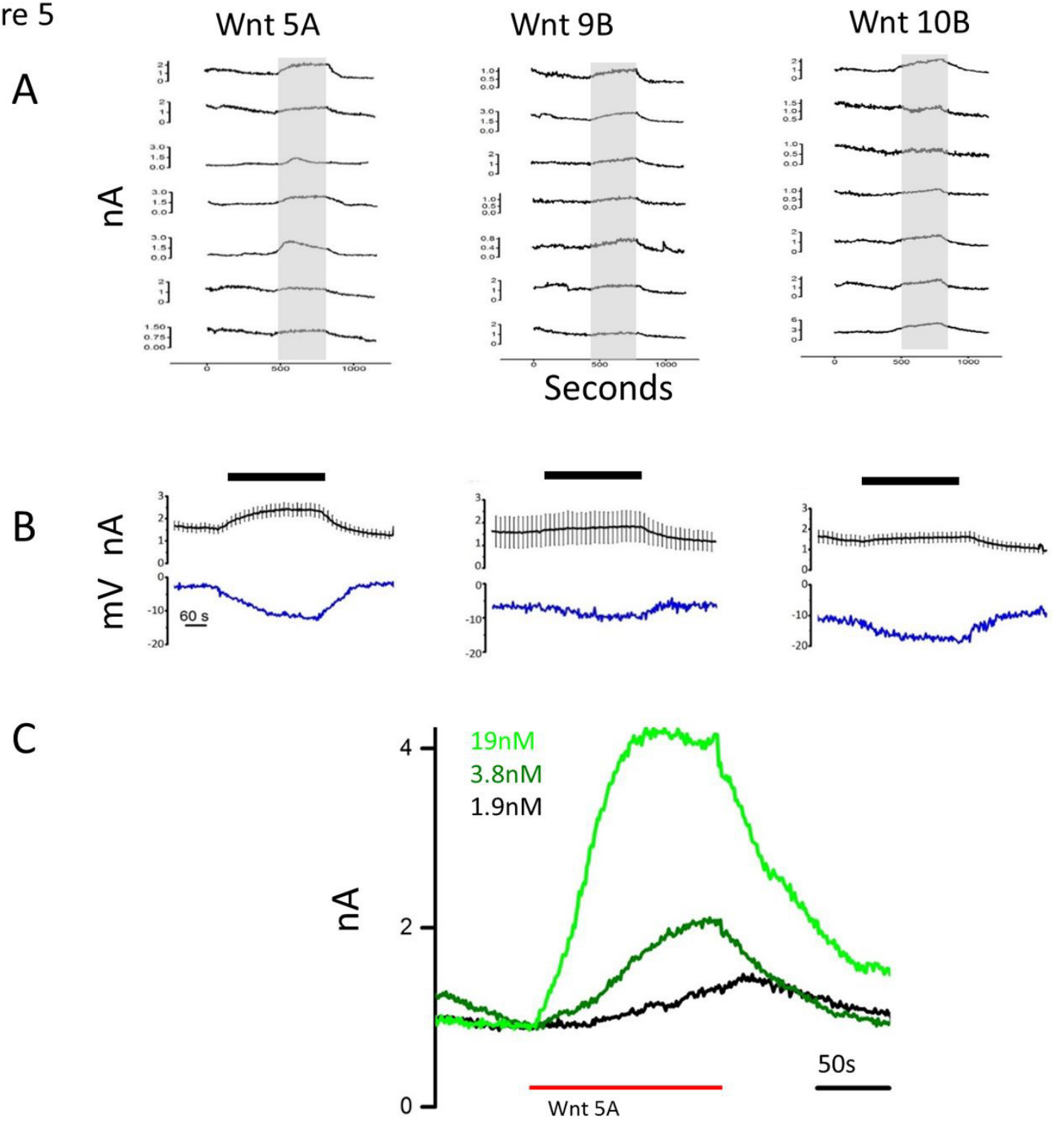
A
Wnt 5A
Wnt 9B
Wnt 10B
nA
Seconds
B
mV nA
60 s
C
19nM
3.8nM
1.9nM
nA
50s
Wnt 5A

Figure 6

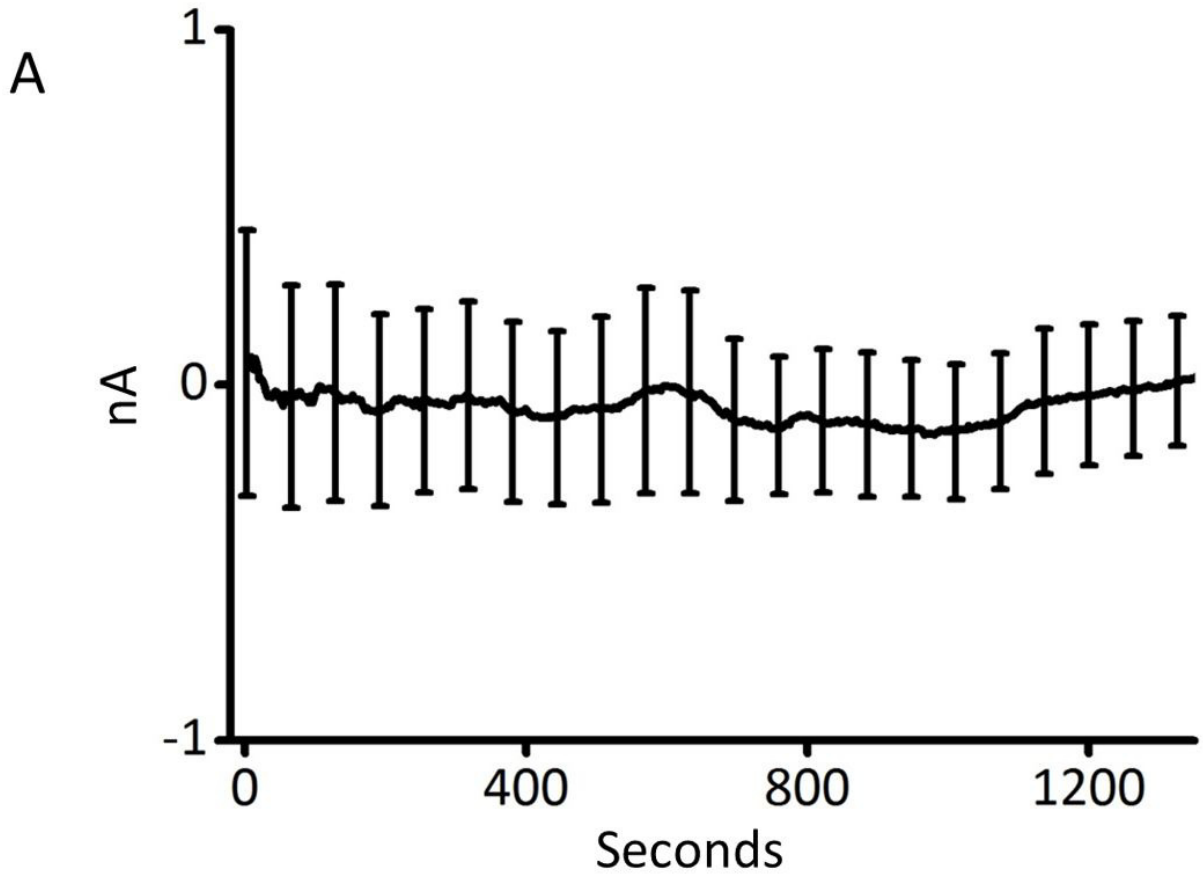
A
1
0
-1
nA
0
400
800
1200
Seconds

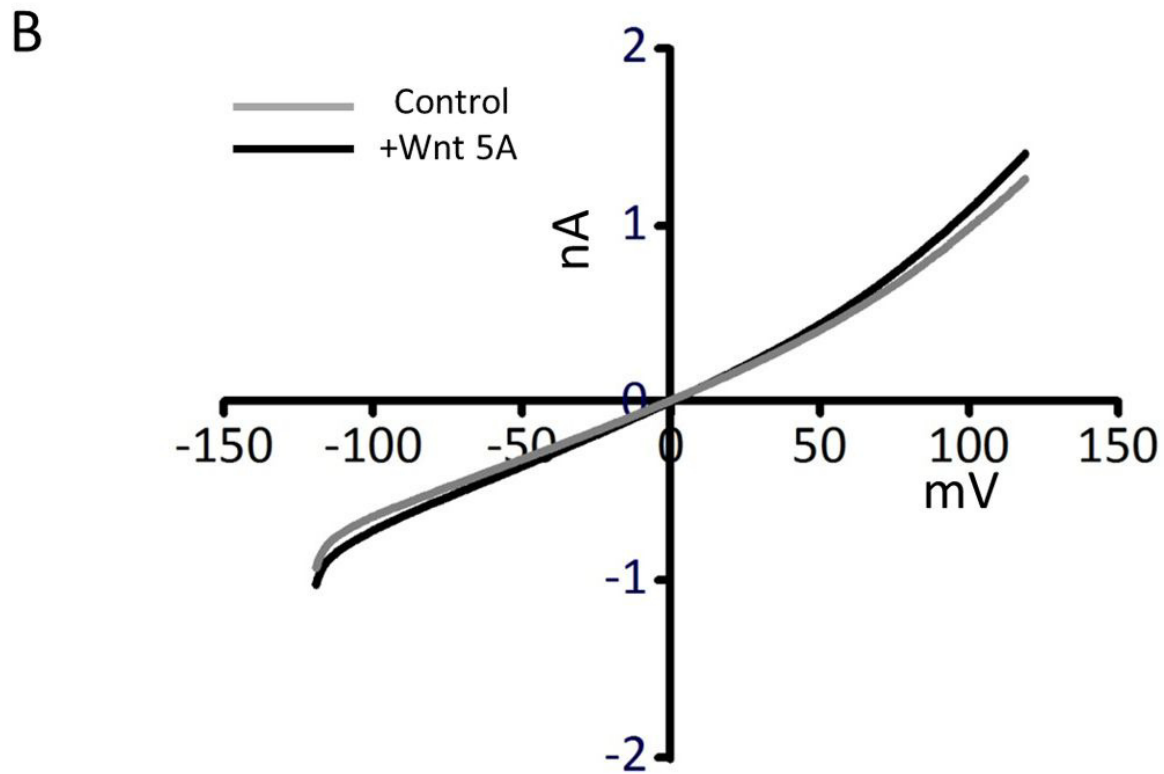
B
Control
+Wnt 5A
2
1
0
-1
-2
nA
-150
-100
-50
0
50
100
150
mV

Figure 7

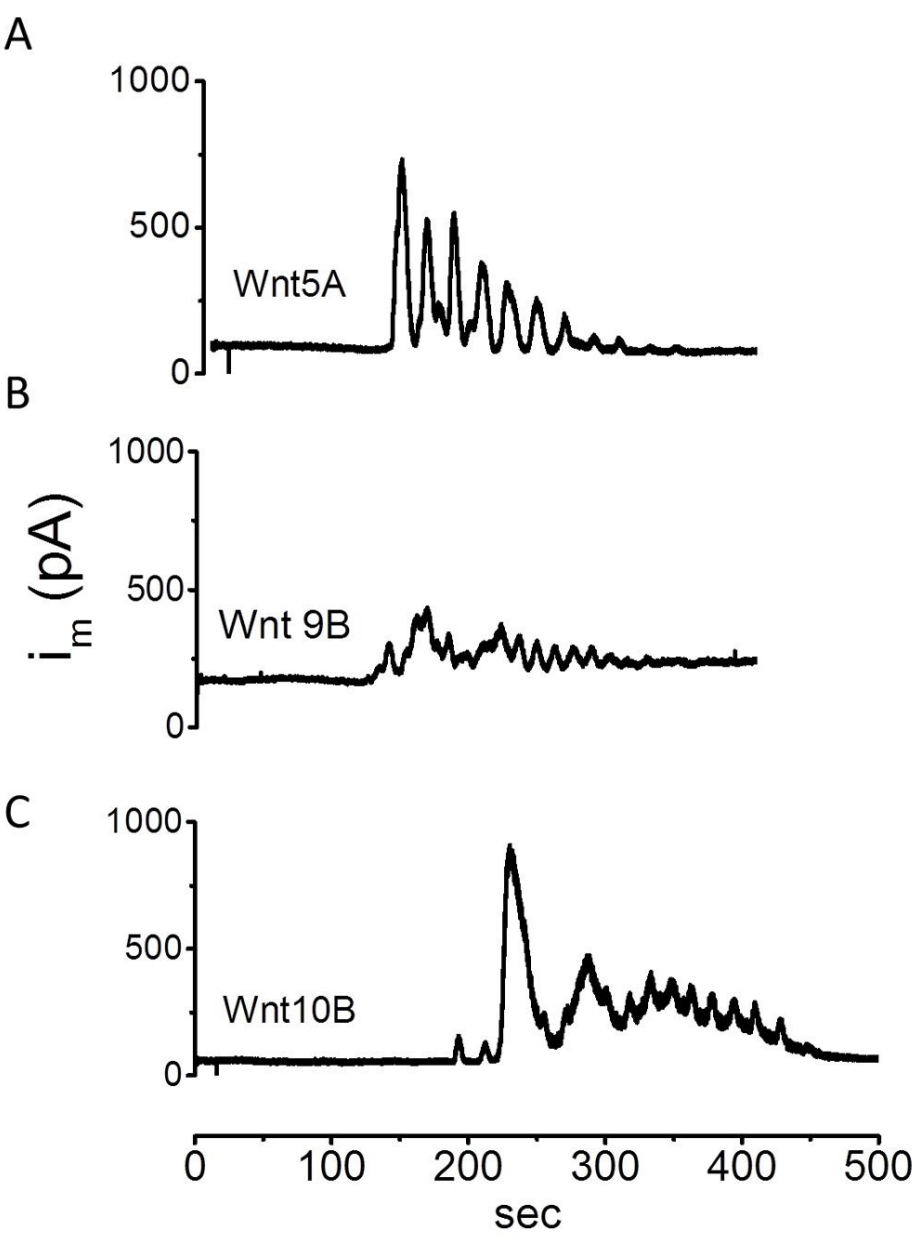
A
1000
500
0
Wnt5A
B
1000
500
0
Wnt 9B
i_m (pA)
C
1000
500
0
Wnt10B
0
100
200
300
400
500
sec

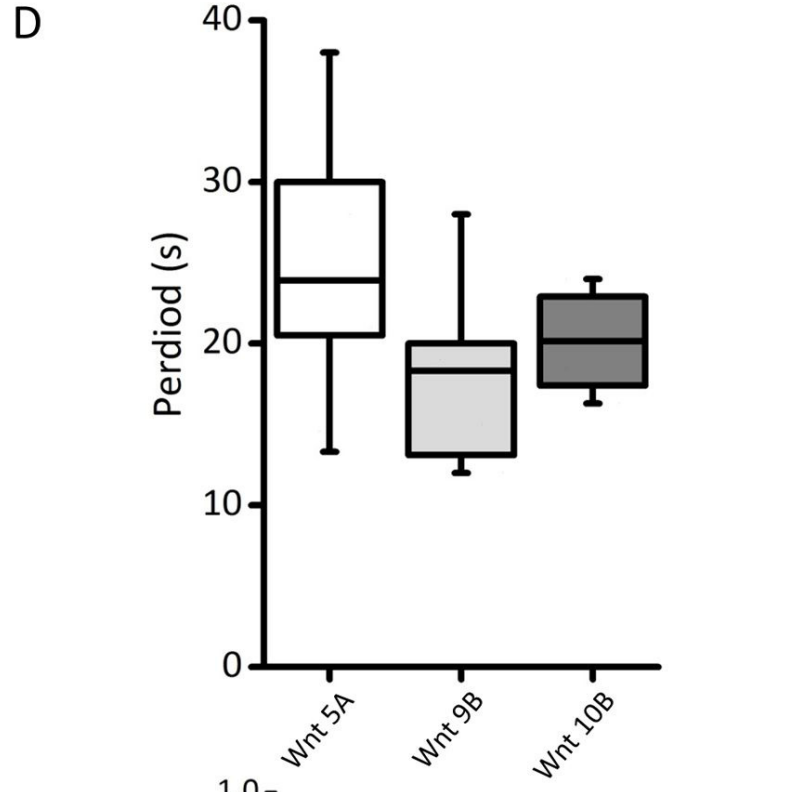
D
40
30
20
10
0
Perdiod (s)
Wnt 5A
Wnt 9B
Wnt 10B

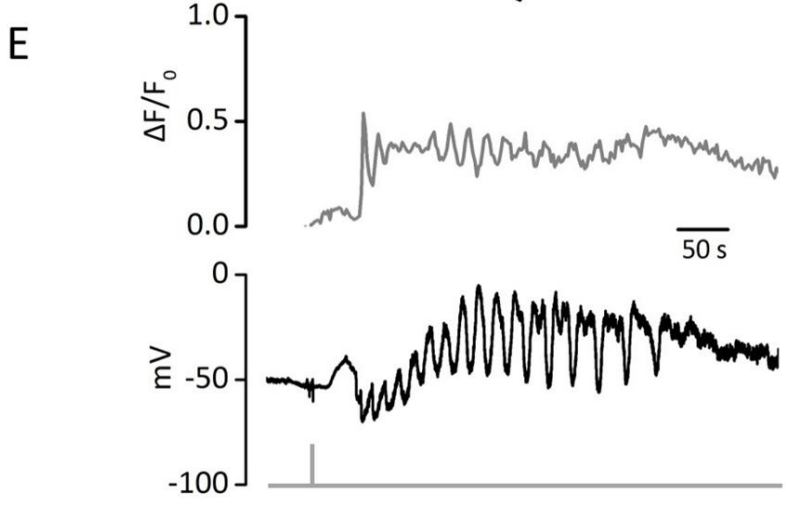
E
1.0
0.5
0.0
$\Delta F/F_0$
50 s
0
-50
-100
mV

Figure 8

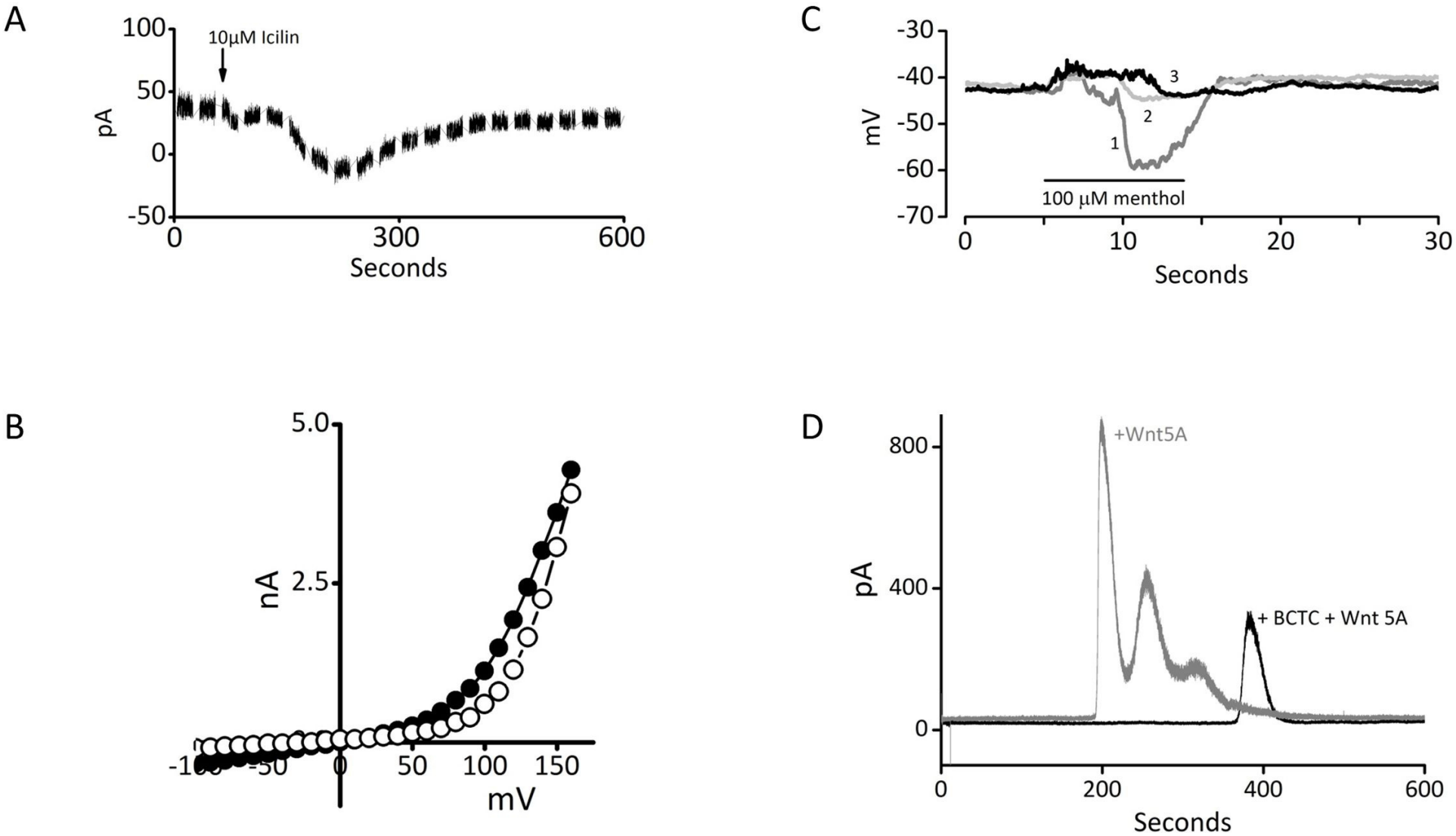
A
10μM Icilin
pA
100
50
0
-50
0
300
600
Seconds
C
mV
-30
-40
-50
-60
-70
1
2
3
100 μM menthol
0
10
20
30
Seconds
B
nA
5.0
2.5
-100
-50
0
50
100
150
mV
D
pA
800
400
0
+Wnt5A
+ BCTC + Wnt 5A
0
200
400
600
Seconds

Figure 9

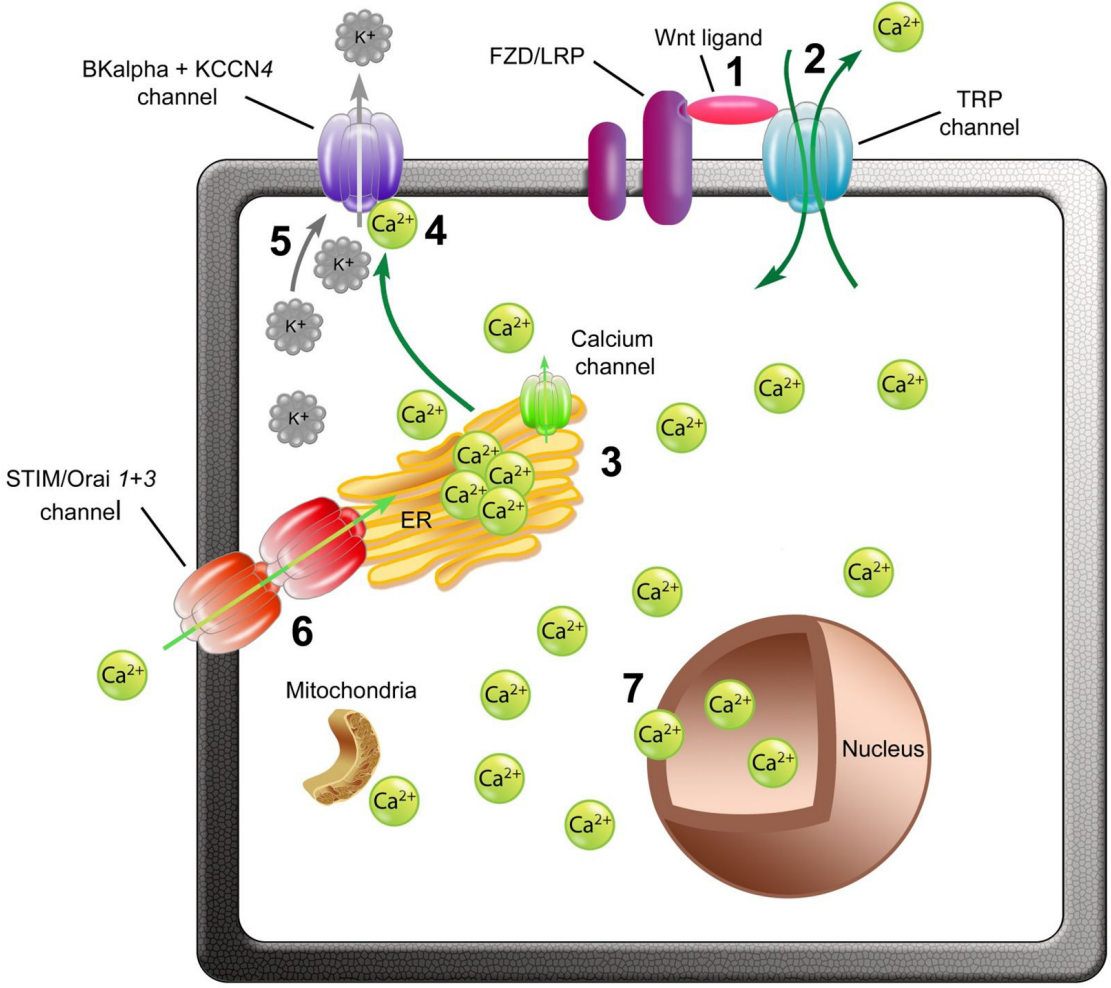
BKalpha + KCCN4 channel
K+
FZD/LRP
Wnt ligand
1
2
Ca2+
TRP channel
5
4
Calcium channel
3
STIM/Orai 1+3 channel
ER
6
Mitochondria
7
Nucleus